1st LATAM-SHM 2023 Conference
A. Güemes, L. Mujica, J. Sierra (Eds)

AUTOMATED MODAL IDENTIFICATION OF OPERATIONAL WIND TURBINE BLADES

FELIPE I. BRAVO*, RODRIGO ASTROZA*, MARCOS ORCHARD†

* Faculty of Engineering and Applied Sciences
Universidad de los Andes
Santiago, Chile
e-mail: fbravo1@miuandes.cl, rastroza@miuandes.cl

† Department of Electrical Engineering
Universidad de Chile
Santiago, Chile
e-mail: morchard@ing.uchile.cl

Key Words: Structural Health Monitoring, Wind Turbine Blades, Environmental and Operational Variability, Modal Analysis

Abstract. This study proposes a continuous-time automated operational modal analysis approach for conducting system identification of wind turbine blades. A vibration-based monitoring system consisting of low-cost microcontrollers and acceleration sensors was designed and deployed in a reduced scale wind turbine mock-up. Vibration data was collected during a long period of time under different environmental and operational conditions and considering several artificially induced damage scenarios. The combined deterministic-stochastic subspace identification method and clustering techniques were used to automatically identify the modal parameters of wind turbine blades. Natural frequencies, damping ratios, and mode shapes of several modes were successfully identified, and the effects of temperature, rotating speed, added masses, and damage conditions on the identified modal parameters are comprehensively discussed.

1 INTRODUCTION

Wind turbines (WTs) are exposed to harsh environmental and operational conditions, making crucial to develop appropriate inspection and maintenance strategies. Complex load characterization, summed to extreme environmental and operational variables (EOV) generate unexpected failures in wind turbines, where wind turbine blades (WTBs) are critical components that have shown a high failure rate [1], and their early damage diagnosis and prognosis is desirable.

In the last decades, vibration-based structural health monitoring (SHM) has gained special interest for damage detection purposes in buildings [2], bridges [3], WTs [4] [5] [6], and other structures. However, a limited number of studies have focused on damage detection of WTBs [7] [8]. Among different strategies for vibration-based SHM, operational modal analysis

(OMA) is desired, since changes in modal properties can reflect damage progressions through vibration derived from the environment and operational sources without interrupting the power generation of the WTs.

Some studies have utilized acceleration data and stress resultant damage detection techniques, which required actuators to excite the blade. However, these techniques were found to be inapplicable in certain cases [9]. Experiments under stationary laboratory conditions have been performed by Ou et al. [10] using vibrations and strain sensors to describe varying temperature, ice accretion-resembling mass, and damage conditions. Signal processing techniques using Power Spectral Density (PSD) analysis and statistical analysis based on Frequency Response Functions (FRF) have been employed [10], while other studies have used state-space identification methods, being the stochastic subspace identification (SSI) algorithm widely employed [11].

This study presents a continuous-time automated modal analysis on the blades of an operational small-scale wind turbine exposed to different operational and environmental variables. The combined deterministic-stochastic subspace identification (DSI) method is used to estimate the modal properties of the blades. By using clustering algorithms, the study shows frequency and damping variations along different ambient temperature, pitch angle, mass addition, and damage progression under varying rotational speeds of the WT to better understand the effect of these variables on the modal properties of the WTBs.

2 METHODOLOGY OVERVIEW

2.1 Experimental setup and monitoring system

An experimental WT was developed to control the operational variables. The test specimen, depicted in Figure 1, is composed by a 3-meter-tall steel tube with a 1 hp motor, a 1:10 reduction gearbox, and a frequency regulator. Three 2.4 meters glass-fiber/epoxy-resin blades are bolted with 10 equally spaced bolts to a hexagonal steel hub.

Figure 1: Experimental wind turbine mock-up

Acceleration measurements were collected by a monitoring device placed at the center of the hexagonal hub. Solar panels and a battery system were used to power a recording device for acceleration and temperature data collection and transmission. Two blades were instrumented with three ADXL345 accelerometers each. The sensors had an amplitude range of ±16 g and a sensitivity of 4 mg/LSB. Acceleration data were recorded at a sampling frequency of 200 Hz and with alternating 10-minute measurement windows. Sensor deployment and blade characteristics are depicted in Figure 2.

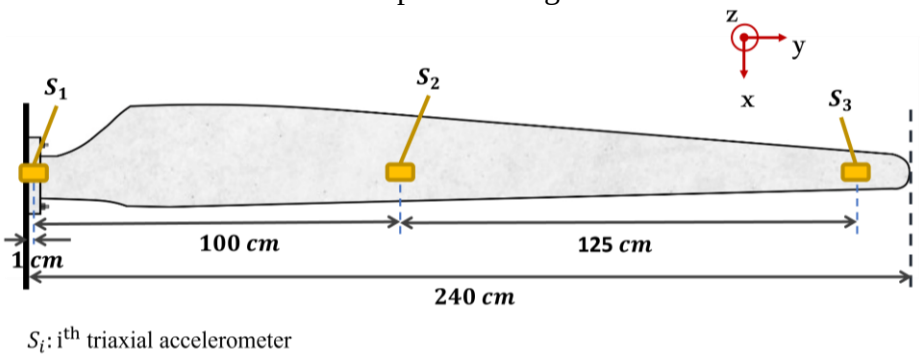

Figure 2: Accelerometer layout in instrumented WTBs

2.2 Automated modal identification

Modal identification of the WTBs was conducted using the DSI algorithm, an input-output system identification method [12]. The method estimates the modal parameters of the WTB from an equivalent linear time-invariant (LTI) state space (SS) model. Discrete-time LTI-SS model as described by Astroza et al. [13] can be expressed as:

$$\begin{aligned} \boldsymbol{x}_{k+1} &= \boldsymbol{A_d} \cdot \boldsymbol{x}_k + \boldsymbol{B_d} \cdot \boldsymbol{u}_k + \boldsymbol{w}_k \\ \boldsymbol{y}_k &= \boldsymbol{C_d} \cdot \boldsymbol{x}_k + \boldsymbol{D_d} \cdot \boldsymbol{u}_k + \boldsymbol{v}_k, \end{aligned} \tag{1}$$

where $\mathbf{x}_k \in \mathbb{R}^n$ = state vector, and n denotes the model order, $\mathbf{y}_k \in \mathbb{R}^l$ = measured output vector (i.e., l = number of outputs), $\mathbf{u}_k \in \mathbb{R}^m$ = input vector (i.e., m = number of inputs), $\mathbf{A} \in \mathbb{R}^{n \times n}$ = state matrix, $\mathbf{B} \in \mathbb{R}^{n \times m}$ = input matrix, $\mathbf{C} \in \mathbb{R}^{l \times n}$ = output matrix, $\mathbf{D} \in \mathbb{R}^{l \times m}$ = direct feed-through matrix, $\mathbf{w}_k \in \mathbb{R}^n$ and $\mathbf{v}_k \in \mathbb{R}^l$ = process and measurement noise vectors, respectively, and k denotes the discrete time instant [12].

The N4SID algorithm was used to estimate the state sequence recovered directly from the input-output data. COM-ALT algorithm was used to solve matrixes **A**, **B**, **C** and **D** [12]. From the relationship between the discrete- and continuous-time state matrices (i.e., $\mathbf{A_d} = \mathrm{e}^{\mathbf{A_c} \cdot \Delta t}$ where $\mathbf{A_c}$ = continuous-time state matrix and Δt = sampling time), it can be shown that their eigenvectors ($\boldsymbol{\Psi}$) are identical, while the eigenvalues of $\mathbf{A_c}$ and $\mathbf{A_d}$ (λ_i and μ_i, respectively) [13] satisfy Eq. (2):

$$\mu_i = e^{\lambda_i \Delta t} \Rightarrow \lambda_i = \frac{\ln(\mu_i)}{\Delta t} \tag{2}$$

From the eigenvalues and eigenvectors of the discrete-time state matrix (A_d) and the discrete-time output matrix (C_d), the natural frequencies (f_i), damping ratios (ξ_i), and mode shapes (ϕ_i) of the system can be obtained as expressed in Eq. (2) to Eq. (4).

$$f_i = \frac{\sqrt{\lambda_i\,\lambda_i^*}}{2\pi} = \frac{|\lambda_i|}{2\pi} \tag{2}$$

$$\xi_i = \frac{-(\lambda_i + \lambda_i^*)}{2\sqrt{\lambda_i\,\lambda_i^*}} = \frac{-\mathrm{Real}(\lambda_i)}{|\lambda_i|} \tag{3}$$

$$\boldsymbol{\Phi} = \mathbf{C_d}\,\boldsymbol{\Psi} = [\boldsymbol{\phi}_1, \boldsymbol{\phi}_2, \dots, \boldsymbol{\phi}_\mathrm{n}\,] \tag{4}$$

The identification process was performed using independent 10-minute-long vibration data windows, referred to as datasets. The root sensor (S1) was considered as input data and the remaining sensors located in the blade (S2 and S3) as output response data (see Figure 2).

Spurious and physical (i.e., normal) mode classification is needed for continuous-time mode tracking. This classification is conducted based on mean phase collinearity (MPC) (Eq. (5)) and mean phase deviation (MPD) (Eq. (6)) indexes with a threshold value λ = 0.7 as suggested by Fan et al. [14]

$$MPC(\phi_j) = \frac{\left\|\mathrm{Re}(\tilde{\phi}_j)\right\|_2^2 + \frac{1}{\epsilon_{MPC}}\mathrm{Re}(\tilde{\phi}_j^T)\mathrm{Im}(\tilde{\phi}_j)(2\epsilon_{MPC}^2 + 1)\sin\theta_{MPC} - 1}{\left\|\mathrm{Re}(\tilde{\phi}_j)\right\|_2^2 + \left\|\mathrm{Im}(\tilde{\phi}_j)\right\|_2^2} \tag{5}$$

$$MPD(\phi_j) = \frac{\sum_{o=1}^{n_y} w_o \arccos\left|\frac{\mathrm{Re}(\phi_{jo})\mathrm{V}_{22} - \mathrm{Im}(\phi_{jo})\mathrm{V}_{12}}{|\phi_{jo}|\sqrt{\mathrm{V}_{12}^2 + \mathrm{V}_{22}^2}}\right|}{\sum_{o=1}^{n_y} w_o}, \quad \sum_{o=1}^{n_y} w_o \neq 0 \tag{6}$$

Then, class grouping is done by similarities in frequency, damping ratio, MPC and mode shape resemblance using the modal assurance criterion (MAC) values (Eq. (7)). The generated classes are then removed if the classified modes are not properly identified in at least 10% of the total number of model orders considered in the identification algorithm. Thresholds values for natural frequency, damping ratio, MPC, and MAC are defined as 1%, 20%, 90%, and 98%, respectively.

$$\frac{\left|\overline{f}_k - f_m\right|}{\overline{f}_k} \leq T_f\ , \qquad \frac{\left|\overline{\xi}_k - \xi_m\right|}{\overline{\xi}_k} \leq T_d\ , \qquad \frac{\left|\overline{MPC}_k - MPC_m\right|}{\overline{MPC}_k} \leq T_{MPC}\ ,$$
$$MAC_{\phi_i,\phi_j} = \frac{\left|\overline{\phi}_i\phi_j\right|^2}{\|\phi_i\|_2^2\|\phi_j\|_2^2}\ , \quad 1 - MAC(\overline{\phi_k}, \phi_m) \leq T_{MAC} \tag{7}$$

Once the modes are classified from the datasets, the mean values of the identified normal modes are compared with existing continuous-time clusters and merged by comparing the mean values of the continuous time cluster frequency, damping ratio, MPC, and mode shape, with the corresponding average results values for every clustered normal mode value of the real time window, where mode shape is compared by MAC index. Clustering merging thresholds used are 2%,100%, 97% and 98% respectively for continuous-time clustering.

If more than one clustered normal mode of the dataset is eligible for the same cluster and merged, using normalized value for frequency and MAC ratio, the nearest distance (Eq. (8)) to the cluster will remain, while the others are neglected.

$$D_{ij} = \frac{|\overline{f}_k - f_m|}{\overline{f}_k} + 1 - MAC(\overline{\phi}_k, \phi_m) \tag{8}$$

2.3 Experimental data

Different cases were considered to assess EOV over one of the wind turbine blades. The cases consider healthy state as reference and go through pitch variations, mass additions, and progressive damage done in the blade (Table 1). Location of added massed and artificially-induced damage (i.e., cuts) are summarized in Figure 3. Vibration data was collected during several days, so the blade was exposed to a wide and representative temperature variations and ambient conditions.

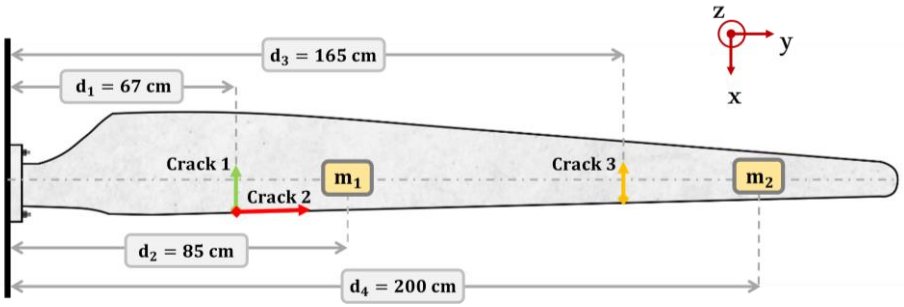

Figure 3: Location of added masses and damage induced in the WTB.

Table 1: Testing protocol and rotating speeds considered in the experiments.

Case	Description			Rotating speed			
R	Healthy state			15rpm	30rpm	45rpm	60rpm
M1	Added Mass m_1=m_2=125g			15rpm		45rpm	
M2	Added Mass m_1=m_2=250g			15rpm		45rpm	
P1	Pitch angle 18°			15rpm			60rpm
P2	Pitch angle 54°			15rpm	30rpm		
P3	Pitch angle 90°			15rpm	30rpm		
D1	Crack 1: l_1 = 2 cm			15rpm	30rpm	45rpm	60rpm
D2	Crack 1: l_1 = 5 cm	Crack 2: l_2 = 2 cm		15rpm		45rpm	
D3	Crack 1: l_1 = 5 cm	Crack 2: l_2 = 2 cm	Crack 3: l_3 = 2 cm	15rpm		45rpm	
D4	Crack 1: l_1 = 5 cm	Crack 2: l_2 = 5 cm	Crack 3: l_3 = 5 cm	15rpm	30rpm	45rpm	60rpm
D5	Crack 1: l_1 = 10 cm	Crack 2: l_2 = 8 cm	Crack 3: l_3 = 5 cm	15rpm		45rpm	
D6	Crack 1: l_1 = 10 cm	Crack 2: l_2 = 8 cm	Crack 3: l_3 = 10 cm	15rpm	30rpm	45rpm	60rpm

3 RESULTS AND DESCUSSION

This section analyzes the effects of temperature, rotating speed, pitch angle of the blade, added masses, and progressive damage on the first flapwise mode of the WTB. The first flapwise mode of the WTB can be used as indicator of health of state of the WTBs as stated by Jaramillo et al. [15]. Identifying mode variations due to EOV is required to accurately isolate the effects of damage on the changes of the modal properties.

3.1 Effect of rotating speed

To analyze the effects of the rotating speed, all other variables must be kept as constant as possible. To this end, the healthy condition without added masses and with 0° pitch angle is considered (i.e., case R in Table 1). To minimize the variability of the temperature, a subset of the data is analyzed, so similar temperature ranges are considered for the different rotating speeds (see Figure 4a). Table 2 summarizes the number of datasets considered in this analysis. A large number of datasets are obtained for different rotating speeds. Figure 4b shows the histogram (i.e., distribution) of the identified natural frequency of the first flapwise mode of the WTB for different rotating speeds. It can be observed that as the speed increases, the natural frequency also does. It is noted that higher rotating speeds increase the deformation of the blade, which in turn increases its stiffness due to nonlinear geometry effects. Figure 4c shows the histogram of the identified damping ratios of the first flapwise mode of the WTB for different rotating speeds. Slight increase of the damping ratio as rotating speed increases is observed at lower rotating speeds (≤45 rpm), while a significant increment can be noted at 60 rpm.

Table 2: Datasets considered in the identification process at the undamaged state of the blade for different rotating speeds in a similar temperature range.

Rotating speed (rpm)	**15 rpm**	**30 rpm**	**45 rpm**	**60 rpm**
# of timeseries	342	549	461	65

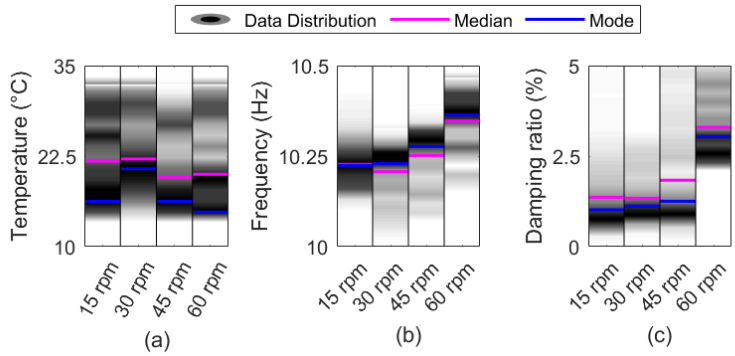

Figure 4: Temperature and system identification results of case R (i.e., healthy with pitch angle 0°) used to analyze the effect of rotating speed, (a) histogram of temperature values, (b) histogram of identified natural frequency of the first flapwise versus rotating speed, (c) histogram of identified damping ratio of the first flapwise mode versus rotating speed.

3.2 Effect of temperature

To study the influence of temperature, the healthy case of the WTB is considered (i.e., case R in Table 1) using all the timeseries recorded. Table 3 summarizes the datasets considered in the analysis. All datasets recorded were considered to obtain the widest temperature range of temperatures possible and considered separately at different rotating speeds. Figure 5a through Figure 5d show linear regressions adjusted to the identified frequencies of the first flapwise mode of the blade versus temperature with high square correlation index along the different rotational speeds. It can be noticed that at higher temperatures the tendency is to

decrease the identified frequency of the first flapwise mode. Additionally, steeper slopes can be noted when increasing rotating speeds. Figure 5e through Figure 5g shows linear regressions adjusted to the identified damping ratio of the first flapwise mode of the blade versus temperature with high square correlation index for rotational speeds higher than 15 rpm. As seen in Figure 5e, a linear regression is not able of properly fitting the relationship at 15 rpm, where other factors seem to be more important than temperature at that rotating speed. On the other hand, linear behavior is observed at higher speeds (≥30 rpm), where at higher rotating speeds, the rise in temperature has a more severe influence in the increase of identified damping ratio of the first flapwise mode response that explains the phenomenon seen in Figure 4c, previously mentioned.

Table 3: Datasets considered in the identification process at the undamaged state for temperature influence.

Rotating speed (rpm)	**15 rpm**	**30 rpm**	**45 rpm**	**60 rpm**
# of timeseries	408	570	501	72

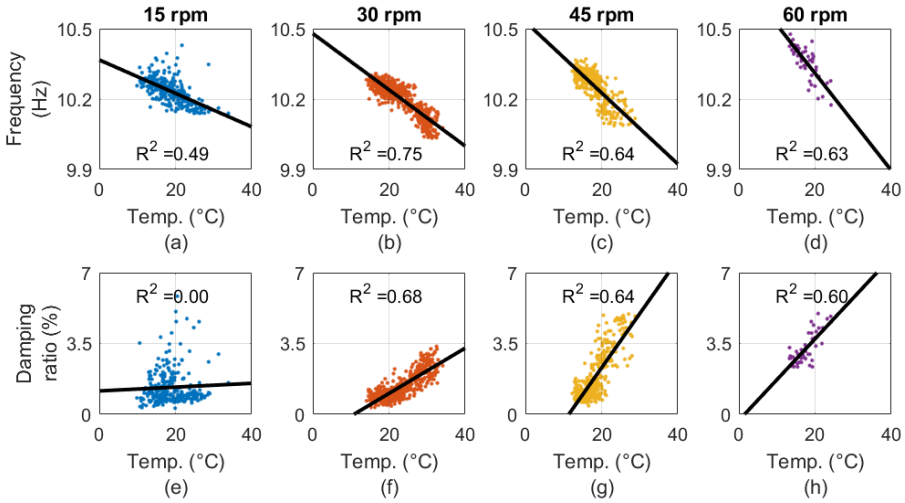

Figure 5: Temperature and system identification results of case R used to analyze the effect of temperature at different rotating speeds, (a, b, c, d) identified natural frequency of the first flapwise mode versus temperature at different rotating speeds, (e, f, g, h) identified damping ratio of the first flapwise mode versus temperature at different rotating speeds.

3.3 Effects of pitch angle

To assess the effect of the pitch angle on the modal properties of the first flapwise mode, all other variables (i.e., temperature, rotating speed, added masses, and damage conditions) were kept fixed or in similar ranges. Vibration data recorded at similar temperatures were considered for different pitch angles (see Figure 6a to Figure 6c) and the results are grouped for different rotating speeds.

Table 4 summarizes the number of datasets considered in this analysis. Figure 6d through Figure 6f shows the histogram of the identified natural frequency of the first flapwise mode of the WTB for different pitch angles at different rotating speeds. Noticeable influence of pitch angle is depicted at the considered rotating speeds, where at 15 rpm (see Figure 6d) a consistent increase in the natural frequency is observed in cases P1 (i.e., pitch angle=18°), P2

(i.e., pitch angle=54°), and P3 (i.e., pitch angle=90°) compared to the refence case (R). Figure 6g through Figure 6i shows the histogram of the identified damping ratios of the first flapwise mode of the WTB for different rotating speeds and pitch angles. No clear effect of the pitch angle on the estimated damping ratios can be observed.

Table 4: Datasets used for the different pitch angles cases at different rotating speeds.

Case label	15 RPM	30 RPM	60 RPM
R	481	505	65
P1	6	-	7
P2	6	6	-
P3	6	6	-

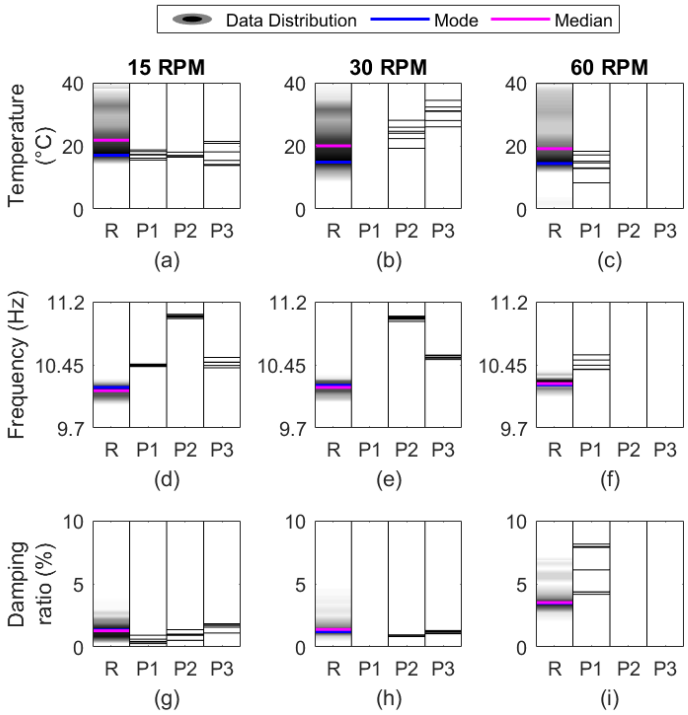

Figure 6: Temperature and system identification results of refence case (i.e., case R) and pitch angle (i.e., cases P1, P2 and P3) used to analyze the effect of pitch angle at different rotating speeds, (a, b, c) histogram of temperature values versus pitch angle cases, (d, e, f) histogram of identified frequency of the first flapwise mode versus pitch angle cases, (g, h, i) histogram of identified damping ratio of the first flapwise mode versus pitch angle at different rotating speeds.

3.4 Effects of added masses

The influence of added masses was studied by comparing the reference case (R) with those cases that included additional masses attached to the WTB (i.e., cases M1 and M2 in Table 1). Since temperature distribution were reasonably close to each other (see Figure 7a and Figure 7b), the whole dataset, as summarized in Table 5, were used in this analysis. Figure 7c and Figure 7d show the histogram of the identified natural frequency of the first flapwise mode of the WTB for the cases with added masses at 15 rpm and 45 rpm, respectively. It can be

observed that mass addition to the blade has a great influence on the natural frequency of the blade, where larger added mass implies lower natural frequency. Compensation effects can be noted when comparing 15 rpm to 45 rpm, where frequency decrease is hidden by the higher rotating speeds. Figure 7e and Figure 7f shows the histogram of the identified damping ratio of the first flapwise mode of the WTB for the cases with added mass at 15 rpm and 45 rpm, respectively. Decreases in damping ratio shown in Figure 7e and increases in damping ratio seen in Figure 7e are most likely due to temperature effects, while no significant influence of mass addition can be reported.

Table 5: Datasets used for the different mass addition cases for considered rotating speeds.

Case label	15 rpm	45 rpm
R	455	501
M1	284	277
M2	286	266

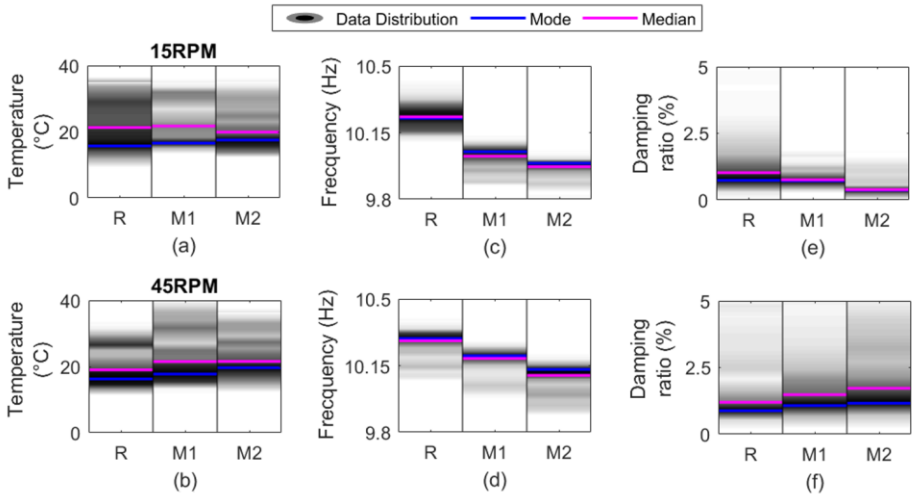

Figure 7: Temperature and system identification results of refence and mass addition cases (i.e., cases R, M1 and M2) used to analyze the effect of mass addition at different rotating speeds, (a, b) histogram of temperature values versus mass addition cases, (c, d) histogram of identified frequency of the first flapwise mode versus mass addition cases, (f, g) histogram of identified damping ratio of the first flapwise mode versus mass addition cases at different rotating speeds.

3.5 Effect of progressive damage

To analyze the effect of damage on the modal properties of the WTBs, it is required to also analyze the possible variations of the temperature, since data cover a wide range of temperatures as can be seen in Figure 8. Table 6 summarizes the number of reference (R) and damaged cases datasets (i.e., cases R, D1, D2, D3, D4, D5, and D6 in Table 1). Figure 9a though Figure 9d shows the histogram of the identified natural frequency of the first flapwise mode of the WTB with different damage cases at different rotating speeds. A considerable influence of temperature is observed on the damage cases response from cases R to D3, where no visible effects on the frequency distribution are detected along the different rotating

speeds. At case D4, the effect of damage begins to be more noticeable, where a decrease in the natural frequency can be seen through D6. Figure 9e to Figure 9h show the histogram of the identified damping ratio of the first flapwise mode of the WTB with different damage cases at different rotating speeds. Effects of temperature and rotating speed are observed, while no clear influence of damage in damping ratio can be seen.

Table 6: Datasets used for the different damage cases for different rotating speeds.

Case label	15 rpm	30 rpm	45 rpm	60 rpm
R	455	570	501	72
D1	481	505	408	65
D2	140	-	236	-
D3	193	-	279	-
D4	453	392	503	146
D5		-	217	-
D6	319	359	362	142

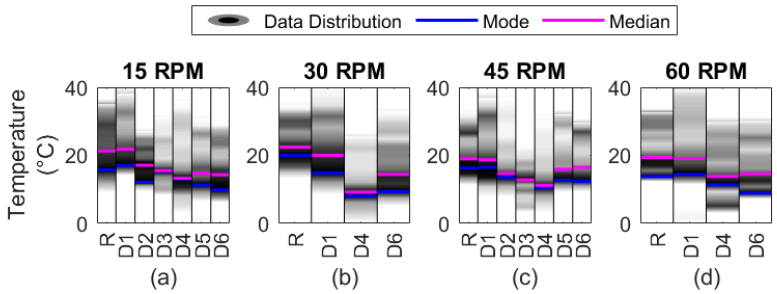

Figure 8: Histogram of temperature values for reference and damage cases (i.e., cases R, D1, D2, D3, D4, D5 and D5) used to analyze the effect of damage at, (a) 15 rpm, (b) 30 rpm, (c) 45 rpm, (d) 60 rpm.

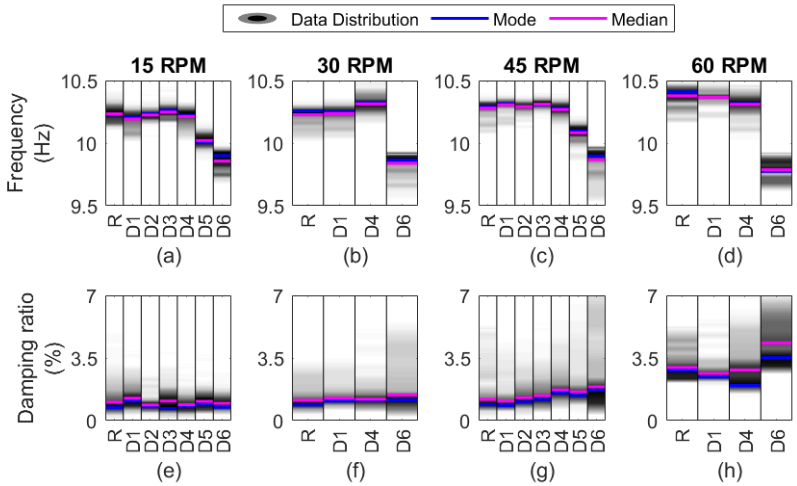

Figure 9: System identification results of for reference and damage cases (i.e., cases R, D1, D2, D3, D4, D5 and D5) used to analyze the effect of damage, (a, b, c, d) histogram identified natural frequency of the first flapwise versus damage cases (e, f, g, h) histogram of identified damping ratio of the first flapwise mode versus damage cases at different rotating speeds.

4 CONCLUSIONS

This study analyzes the effects of environmental and operational variables (EOV), added masses, and damage on the modal properties of wind turbine blades (WTBs). To this end, a monitoring system was developed to record acceleration response data on a 2.4 m long WTBs mounted on a wind turbine mock-up. The deterministic-stochastic subspace identification (DSI) algorithm and clustering techniques were used to automatically estimate the modal properties (i.e., natural frequencies, damping ratios, and mode shapes) of the WTB. The results obtained by the continuous-time automated modal analysis system were then comprehensively analyzed, specifically, the modal parameters of the first flapwise vibration mode of the blade.

The identification results showed that at higher rotating speeds the natural frequency increased. It was observed that the frequency tends to decrease as temperature increased. In addition, at higher speeds, the temperature effects tend to be more noticeable than at lower speeds. Pitch angle showed greater influence than rotating speed and temperature, with frequency values increasing as pitch angle goes from 0° to 54°, while at 90° similar modal parameters as those identified at 18° were obtained. Added masses also influence the identified natural frequency, with larger added masses decreasing the frequency. Finally, artificially-induced damage showed noticeable effects only at final damage states, while when smaller cuts were induced on the blades, no significant effects of the natural frequency were observed.

Damping ratio response of the first flapwise mode of the blade was greatly influenced by temperature and rotating speeds, while no visible effect was observed for pitch angle variations, mass addition, and damage progression. Increases in rotating speed or temperature showed an increase in damping ratio, while temperature effects over amping ratio seems not greatly influential at 15 rpm, while increasingly considerable at higher rotating speeds.

ACKNOWLEDGMENTS

The authors acknowledge the funding from the Chilean National Agency for Research and Development (ANID) through the Fondo de Fomento al Desarrollo Científico y Tecnológico (FONDEF) under Grant ID17I20140. M. Orchard also acknowledges the support from the Advanced Center for Electrical and Electronic Engineering (AC3E), Basal Project FB0008.

REFERENCES

[1] D. A. Katsaprakakis, N. Papadakis and I. Ntintakis, "A comprehensive analysis of wind turbine blade damage," *Energies*, vol. 14, no. 18, p. 5974, 2021.

[2] R. Astroza, H. Ebrahimian, J. Conte, J. Restrepo and T. Hutchinson, " System identification of a full-scale five-story reinforced concrete building tested on the NEES-UCSD shake table," *Structural Control and Health Monitoring*, vol. 23, no. 3, p. 535–559, 2016.

[3] D. Siringoringo and Y. Fujino, "System identification of suspension bridge from ambient vibration response," *Engineering Structures*, vol. 30, no. 2, pp. 462-477, 2008.

[4] P. Cross and X. Ma, "Nonlinear system identification for model-based condition

monitoring of wind turbines," *Renewable Energy,* vol. 71, p. Renewable Energy, 2014.

[5] C.-H. Loh, K. Loh, Y.-S. Yang, W.-Y. Hsiung and Y.-T. Huang, "Vibration-based system identification of wind turbine system," *Structural Control and Health Monitoring,* vol. 24, no. 3, p. e1876, 2016.

[6] C. Devriendt, F. Magalhães, W. Weijtjens, G. De Sitter, A. Cunha and G. Guillaume, "Structural health monitoring of off-shore wind turbines using automated operational modal analysis," *Structural Health Monitoring,* vol. 13, pp. 644-659, 2014.

[7] J. Pacheco-Chérrez, D. Cáardenas, A. Delgadoa and O. Probst, "Operational modal analysis for damage detection in a rotating wind," *Composite Structures,* vol. 321, p. 117298, 2023.

[8] P. Kaewniam, M. Cao, N. Alkayem, D. Li and E. Manoach, "2022 - Recent advances in damage detection of wind turbine blades: A state-of-the-art review," *Renewable and Sustainable Energy Reviews,* vol. 167, p. 112723, 2022.

[9] M. D. Ulriksen, D. Tcherniak, L. M. Hansen, R. J. Johansen, L. Damkilde and L. Froyd, "In-situ damage localization for a wind turbine blade through outlier analysis of stochastic dynamic damage location vector-induced stress resultants," *Structural Health Monitoring,* vol. 16, no. 6, pp. 745-761, 2017.

[10] Y. Ou, V. K. Dertimanis, E. N. Chatzi and M. D. Spiridonakos, "Vibration-based experimental damage detection of a small-scale wind turbine blade," *Structural Health Monitoring,* vol. 16, no. 1, pp. 79-96, 2017.

[11] D. Augustyn, N. Cosack and M. D. Ulriksen, "On the influence of environmental and operational variability on modal parameters of offshore wind support structures," *Marine Structures,* vol. 84, p. 103185, 2022.

[12] P. Van Overschee and B. De Moore, Subspace identification for linear systems: Theory—Implementation—Applications., First ed., NY: Springer New York, 1996.

[13] R. Astroza, H. Ebrahimian, J. P. Conte, J. I. Restrepo and T. C. Hutchinson, "Statistical analysis of the modal properties of a seismically-damaged five-story RC building identified using ambient vibration data," *Journal of Building Engineering,* vol. 52, p. 104411, 2022.

[14] G. Fan, J. Li and H. Hao, "Improved Automated operational modal identification of structures based on clustering," *Structural Control and Health Monitoring,* vol. 26, no. 12, p. e2450, 2019.

[15] F. Jaramillo, J. Gutiérrez, M. Orchard, M. Guarini and R. and Astroza, " A Bayesian approach for fatigue damage diagnosis and prognosis of wind turbine blades," *Mechanical Systems and Signal Processing,* vol. 174, p. 109067, 2022.